Lyes Azzouz, Yong Chen, Mauro Zarrelli, Joshua M.Pearce, Leslie Mitchell, Guogang Ren, Marzio Grasso. Mechanical properties of 3-D printed truss-like lattice biopolymer non-stochastic structures for sandwich panels with natural fibre composite skins, *Composite Structures* 213:220-230 (2019).https://doi.org/10.1016/j.compstruct.2019.01.103

Mechanical properties of 3-D printed truss-like lattice biopolymer non-stochastic structures for sandwich panels with natural fibre composite skins

Lyes Azzouz[1], Yong Chen[1], Mauro Zarrelli[2], Joshua M. Pearce[3,4], Leslie Mitchell[1], Guogang Ren[1*], Marzio Grasso[1*]

1. Automotive, Mechanical and Mechatronics Engineering Division, School of Engineering and Technology, University of Hertfordshire m.grasso@herts.ac.uk; g.g.ren@herts.ac.uk

2. National Research Council Italy – CNR Institute for Polymers, Composites and Biomaterials IPCB, Italy

3. Department of Material Science & Engineering and Department of Electrical & Computer Engineering, Michigan Technological University, Houghton, MI

4. Department of Electronics and Nanoengineering, School of Electrical Engineering, Aalto University, Espoo, Finland

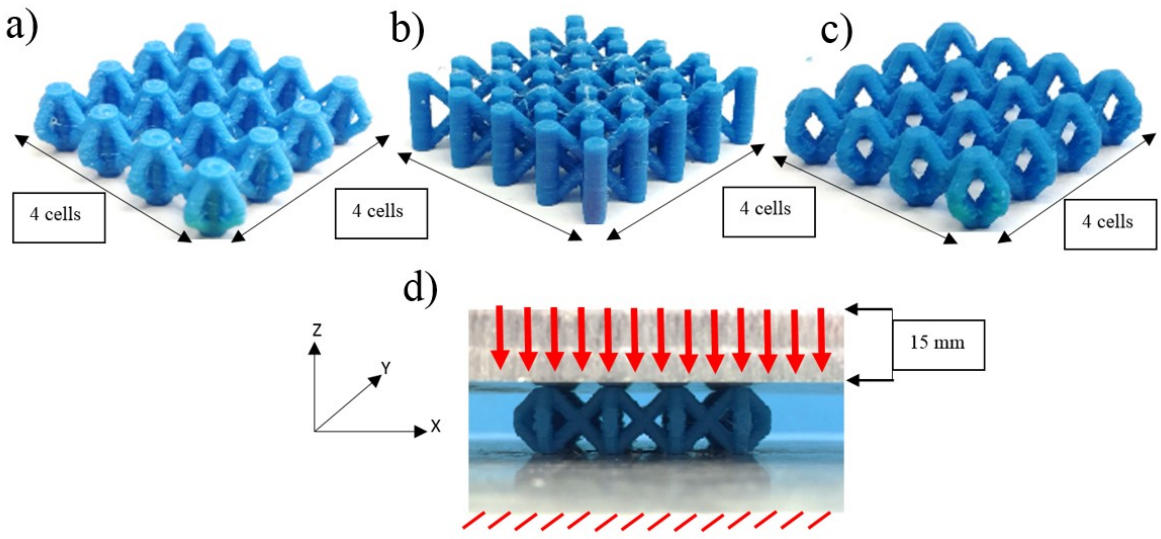

Lyes Azzouz, Yong Chen, Mauro Zarrelli, Joshua M.Pearce, Leslie Mitchell, Guogang Ren, Marzio Grasso. Mechanical properties of 3-D printed truss-like lattice biopolymer non-stochastic structures for sandwich panels with natural fibre composite skins, *Composite Structures* 213:220-230 (2019).https://doi.org/10.1016/j.compstruct.2019.01.103

Abstract

A full mechanical characterisation of three types of 3-D printed lattice cores was performed to evaluate the feasibility of using additive manufacturing (AM) of lightweight polymer-based sandwich panels for structural applications. Effects of the shape of three selected lattice structures on the compression, shear and bending strength has been experimentally investigated. The specimens tested were manufactured with an open source fused filament fabrication-based 3-D printer. These sandwich structures considered had skins made of polypropylene (PP)-flax bonded to the polylactic acid (PLA) lattice structure core using bi-component epoxy adhesive. The PP-flax and the PLA core structures were tested separately as well as bonded together to evaluate the structural performance as sandwich panels. The compression tests were carried out to assess the in-plane and out of plane stiffness and strength by selecting a representative number of cells. Shear band and plastic hinges were observed during the in-plane tests. The shear and three-point bending tests were performed according to the standard to ensure repeatability. The work has provided an insight into the failure modes of the different shapes, and the force-displacement history curves were linked to the progressive failure mechanisms experienced by the structures. Overall, the results of the three truss-like lattice biopolymer non-stochastic structures investigated have indicated that they are well suited to be used for potential impact applications because of their high-shear and out of the plane compression strength. These results demonstrate the feasibility of AM technology in manufacturing of lightweight polymer-based sandwich panels for potential structural uses.

Lyes Azzouz, Yong Chen, Mauro Zarrelli, Joshua M.Pearce, Leslie Mitchell, Guogang Ren, Marzio Grasso. Mechanical properties of 3-D printed truss-like lattice biopolymer non-stochastic structures for sandwich panels with natural fibre composite skins, *Composite Structures* 213:220-230 (2019).https://doi.org/10.1016/j.compstruct.2019.01.103

Keywords: natural fibre composites, lattice structures, PLA, sandwich structure, stochastic structures, biopolymers

1. Introduction

Sandwich structures are advantageous for structural applications exhibiting low-weight, high-stiffness and high energy absorption [1-3]. Depending on the industry standards and functional requirements, sandwich cores come in different forms and materials including honeycomb and metals for aerospace [4, 5] and marine applications [6], natural composites [7] foam, balsa and wood for automotive [2] and many other applications including construction [8]. Sandwich panels consists of two thin face sheet skins contributing to the flexural stiffness of the panel, whereas the core is responsible for the shear transfer between the skins. The core can also contribute to the overall flexural and compressive strength of the panel. Cellular core sandwich structures have been developed for various structural requirements in order to develop lightweight and adequately stiff and strong composites. Advancement in additive manufacturing (AM) technology has led to the emergence of metallic core in the form of cellular honeycomb structures and truss-like structures specifically for high-performance mechanical properties typically used in lightweight energy absorbing products [9-12] . Much attention and development activities have been dedicated to produce optimised metallic structures through improved designs and build parameters [13]. There is a potential to use cellular honeycomb structures in polymer applications as well, but reinforced polymers and polymer composites would be preferred for improved mechanical strength. A comprehensive study by Yazdani et.al. [14] covered the theoretical,

numerical and experimental aspects of the geometry optimisation of 3D printed cellular cores for energy absorption applications.

Bio-composite materials offer the promise to improve sustainability and functionality compared to oil-derived polymer materials. 3-D printing (3DP) these materials for future applications because of geometric flexibility (e.g. honeycomb lightweight structures) is of particular interest [15]. Natural fibre (NF)-based composites have recently attracted interest due to the increased ecological concerns in global industry since issues of manufacturing-based energy burdens, recyclability and environmental safety become the centre of new materials and products developments [16, 17] . Among these natural fibres, lignocellulosic bast-fibres such as flax, hemp and jute are widely used for reinforcement of thermoplastic polymers. The reinforcement of renewable sourced polymers with flax fibres is encouraged due to their low density, good mechanical properties and low environmental impact. Flax and polypropylene (PP) has been shown to be compatible for making high-quality composites [18] . Although PP can be printed, it is more challenging than the natural polymers polylactic acid (PLA), which is the most common fused filament fabrication (FFF)/fused deposition modelling (FDM) 3-D printed polymer. Due to its low melting temperature and ease of printing PLA can even be used by consumers to make finished products [19]. The mechanical properties of FFF/FDM PLA are well established [20-23], and their chemical resistance is also known [24]. PLA has also been successfully used in a number of polymer matrix composites [25-30].

These advances in sandwich structures and polymer/natural fibre composites open up the potential to overcome one of the primary limitations of FFF/FDM in load bearing applications: highly anisotropic properties having particularly low stiffens and strength in the direction of layer deposition (z-direction) [31-34]. A review by Ngo et al. [35] summarised the main methods commonly utilised in additive manufacturing among which FDM was discussed. In FFF/FDM three dimensional parts directly imported from CAD models are fabricated based on the deposition of melted filaments to create an object as a composition of several overlapping layers, where each layer is composed of a continuous bead extruded and deposited which solidifies by cooling [31]. Amongst the complex geometries that can be produced using FFF/FDM is the lattice or cellular structure for load-bearing applications, and it is expected that the mechanical properties of the sandwich cellular structures for load-bearing applications could be improved by fibre reinforced thermoplastics.

In order to probe these potentials, a study was designed to take advantage of the more advanced work in PP-flax composites to make up the top and bottom layer of the sandwich structure and PLA to form 3-D printed truss-like lattice units of a non-stochastic structures making up the internals. The aim of this work thus was to collect sufficient mechanical properties of three selected lattice topologies of PLA and PP+flax composites to be used in the structure optimisation process for sandwich structures. Mechanical tests included compression both in-plane and out-of-plane (edgewise and flatwise), core shear and sandwich flexural. Force vs displacement curves were generated, which were then processed

accordingly to interpret the achieved results and later discussed the overall response to draw conclusions on stress distributions within the structures and identify high-stress regions which may require reinforcement and low-stress regions where with potential weight savings. The potential for FFF/FDM to provide load-bearing structures for various applications with these materials are discussed, and conclusions are drawn.

2. Materials and methodology

2.1. Lattice structures

Cellular solids are divided into two main groups: 1) stochastic structures (or foams) are classified according to their porosity type open-cell or closed-cell, whereas 2) the non-stochastic are categorised according to their building unit cell either 2-D lattice unit (honeycomb) or 3-D lattice unit (truss-like) [36]. The lattice structure is a truss-like structure with a repeating unit cell that forms intersecting struts and nodes with a specific recurring arrangement over a volumetric region. The internal design of these struts whether hollow, circular, square or any desired shape cross sections is application dependent and more specifically dependent on the strength and stiffness requirements [37] . Kagome truss core structures perform better than conventional honeycomb core structures in terms of their specific compressive and shear strength. In order to maximise the compressive and shear strength of the kagome structure, the internal angle can be adjusted closer to 45° or 60° respectively. The three unit cell structures were developed with the CAD software CATIA V5 (Dassualt Systemes, Velizy-Villacoublay, France), motivated from the previously investigated structures in literature. However modifications to the geometry and dimensions

have been applied to improve the print quality and reduce manufacturing times. Lattice structures are generated by repeating unit cells, which are cylindrical struts built at different orientations connected through nodes. For comparison purposes a fixed envelop of width and height of 10 x10 mm is used. The STL files of the designs can be found at the Open Science Framework [38] and are shown in **Figure 1.**

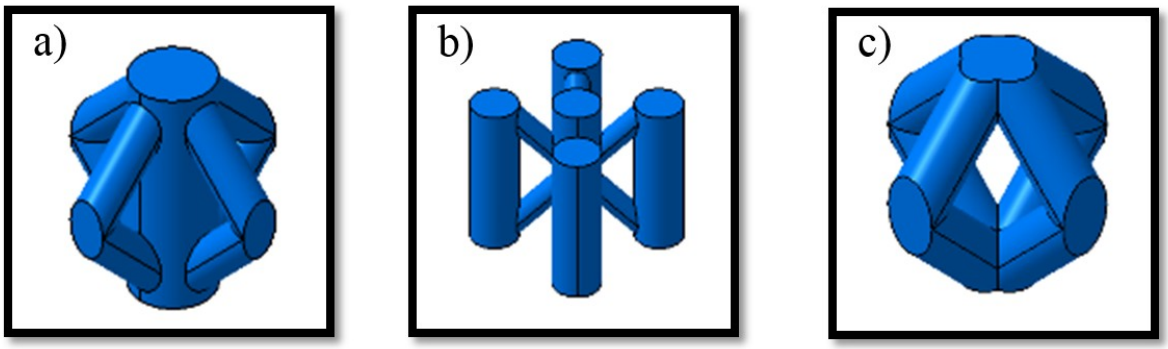

Figure 1 - a) Lattice 1: BCC-Z structure, b) Lattice 2: circumferential rectangular pattern of 4 vertical struts and c) Lattice 3: BCC unit cell without the vertical strut.

Lattice 1 is a diamond design that has a vertical strut that runs through the middle of the unit cell. The vertical strut in the centre of the cell has a diameter of 2.5 mm whilst the remaining diagonal struts have a reduced thickness of 1.5 mm. With the vertical strut present in the layout of the unit cell, the compressive capabilities of the cell should see greater improvement compared to the same design without. For the second unit cell, a cube-like format has been utilised, with five vertical struts (4 on each corner with 1 in the centre), and eight smaller struts that meet at the middle of the vertical strut in the centre of the cell. Similar to unit cell 1, the vertical struts have a thickness of 2.5 mm whereas the smaller diagonal strut bear a thickness of 1.5 mm. This cell structure is expected to perform especially well under compression due to an increase in mass as a result of the additional

vertical struts in comparison to unit cell 1. The third unit cell to be observed is a cell that also takes a diamond form like that of unit cell 1. However, it differs in the fact that it does not have the vertical strut present in the centre of the cell. As a result, it is expected to perform to a lower standard to unit cell 1 under compression. Due to the absence of vertical struts in this cell, the thickness of the struts is marginally thicker than the other two cells, with a diameter of 2 mm instead of the original 1.5 mm.

2.2. Manufacturing

Manufacturing of specimens was carried out using an open source Ultimaker 3 Extended dual extruder (Ultimaker, the Netherlands) equipped with 0.4 mm nozzles on a 215 x 215 mm heated glass build plate. CAD files were imported into Cura 2.7.0 [39] in STL format to be sliced, and a list of printing parameters was adjusted accordingly. These instructions are subsequently generated in a G-code script, which the printer uses to perform the printing. A process of fine-tuning the printing parameters to attain an optimum quality where a visual investigation of printed parts was carried out to identify physical defects, which could potentially yield inconsistent results following [40]. No support material was used for all printing operations in order to make this method of manufacturing sandwich structures realistic in mass production. In addition printing without support reduces energy and materials, which reduces costs as well as environmental impact.

The complete list of parameters used to 3-D print all types of specimen is shown in **Table 1**.

Table 1 - 3-D printing parameters used to manufacture the samples tested in this work.

Layer Thickness (mm)	0.1
Infill density (%)	100
Print temperature (°C)	225
Build bed temperature (°C)	60
Print speed (mm/s)	15
Flow rate (%)	100
Build bed adhesion	Glue stick

2.3 Materials

The feedstock for the 3-D printed cores used in this study was a PLA filament made of starch promoting its biodegradability and biocompatibility. Spools of blue PLA 750 g of 2.75 mm diameter, melting temperature range of 145 -160°C and a specific density of 1.24 purchased from RS Components Ltd, UK. The mechanical properties of bulk PLA were reported in the datasheet [41] with a tensile modulus of 2852 MPa and yield stress of 38.5 MPa, which were tested in accordance with ISO 527.

Natural fibre composites (NFC) face sheets made of discontinuous flax fibres and polypropylene and preformed with a mass content ratio 52:48 Flax/PP were produced at EcoTechnilin Ltd, Cambridgeshire, UK. These consolidated mats called fibriplast sheets are a mixture of discontinuous flax fibres, and PP interlocked using needle punch process with 30,000 needles/s resulting in the aerial weight of 1200 gsm. Consolidation using heated press with applied pressure of 20 MPa and 120°C temperature for 5 minutes yield a reduced thickness of 2 mm. The motivation for the use of NFC as opposed to the use of virgin polypropylene is the eco-friendliness of flax fibres and reduced carbon footprint.

Furthermore, polypropylene is a fossil fuel based thermoplastic with a maximum tensile modulus of 1.5 GPa and strength of 30 MPa [42].

For the sandwich panel's production, the adhesion of the 3-D printed core to the NF face sheets was achieved using Araldite 2015 (AV5308/ HV5309-1) bi-component epoxy paste adhesive purchased from RS Components Ltd, Northants, UK. The two-part epoxy resin and hardener were mixed in an equal amounts and allowed to react for 5 minutes in room temperature before being applied on the face sheets only.

2.4 Mechanical testing

2.4.1 Tensile testing of NFC

The tensile properties (i.e. stiffness and strength) of NFC were evaluated in accordance with ISO 527-4:1997 and standard test specimen type 1B with no end tabbing using the electromechanical testing Tinius Olsen 25 ST with 25 kN load cell (**Figure 2)**. Tests were performed on specimen of 150 x 20 x 2 mm in dimension at a crosshead displacement of 2 mm/min and gauge length of 50 mm of a reduced width of 10 mm. Tests were carried out at room temperature, and at least three repetitions were performed, and raw results were averaged to a mean value with Tinius Olsen Horizon software**.**

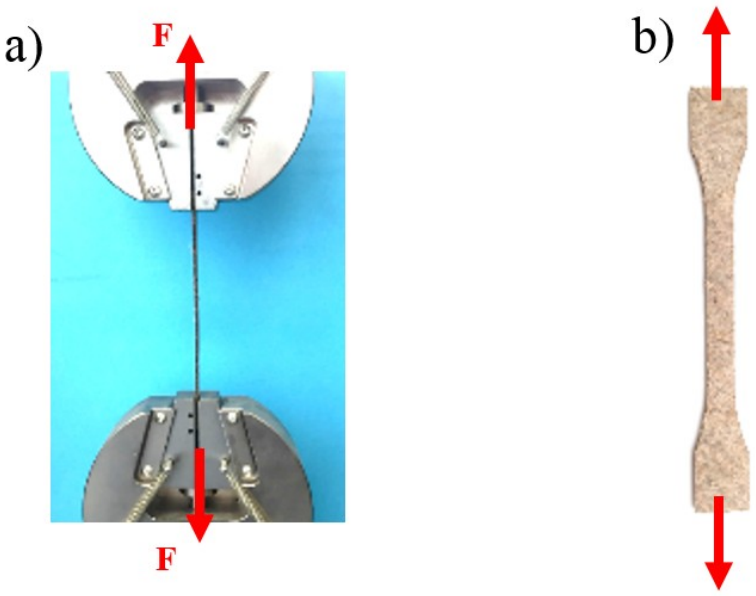

Figure 2 - a) Tensile test set up for the NFC, b) flax/ PP specimen geometry.

2.4.2 Compression testing of core lattice structures

Quasi-static compression tests in-plane and out-of-plane were performed on the three core lattice structures using the same Tinius Olsen 25 ST machine. In-plane test also called edgewise compression is a method to determine the compressive strength and stiffness in the direction parallel to the sandwich facing plane. Specimens tested were only lattice cores without face sheets therefore buckling was insignificant. These tests were constructed to replicate the ASTM C364-99 standard as closely as possible with some modifications to the geometry for clamping purposes. Dimensions of the cubic tested specimen were dependent on the unit cell dimensions however for comparison purposes the number of cells was chosen as 4 x 4 x 1 cells in the x, y and z directions, respectively as shown in **Figure 3**. Nominal dimensions and weights were verified for each specimen before carrying out compression tests. For the compression tests the crosshead displacement rate was set at 1 mm/min, load cell recording the applied force. The out-of-plane or flatwise compressive testing consists of

subjecting the three lattice structures to a uniaxial load in the z-direction normal to the plane of the face sheets. Since the top and bottom of specimen are flat, the loading platens transmit the force with no geometrical modifications. Whereas strut brackets like on the Lattice 1 and 3 specimen edges have been sanded down to create a flat surface on both the bottom and top ends on which the loading platens rest as illustrated in **Figure 4.**

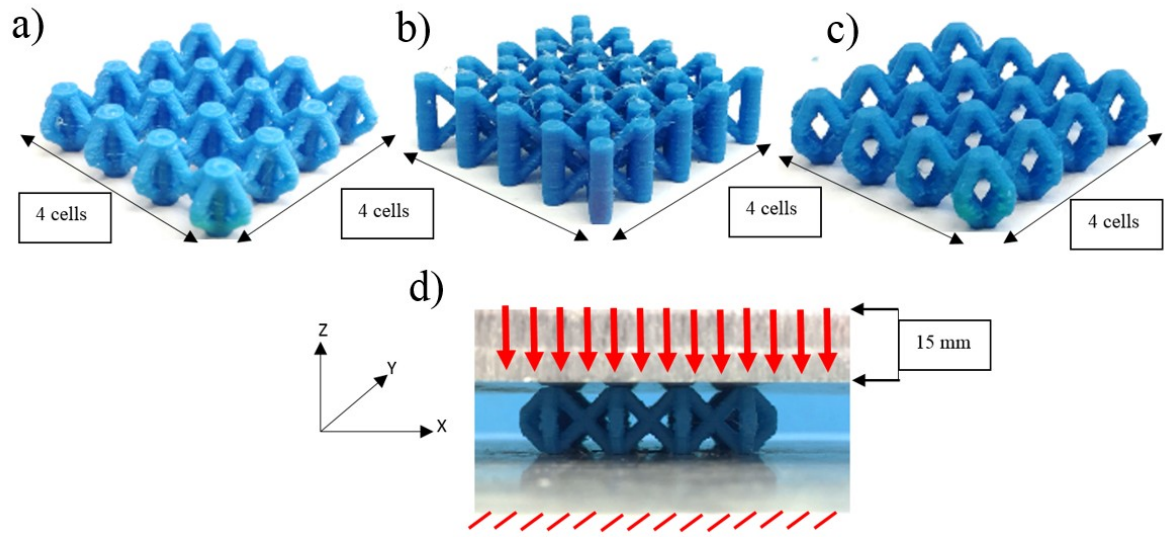

Figure 3 - 3D printed PLA cellular lattice fabricated for compression test: a) Lattice 1, b) Lattice 2, c) Lattice 3, d) out-of-plane compression test set up.

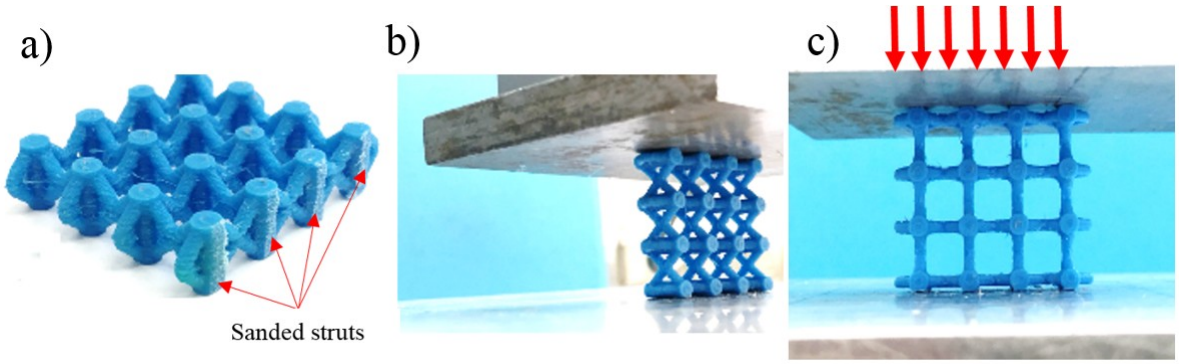

Figure 4 - In-plane compression test set up: a) inclined struts sanded down, b) perfect alignment, c) load line direction with specimen under testing.

2.4.3 Shear testing of core lattice structures

A customised shear test set up fixture was designed to replicate the procedure described in the ASTM C273-00. Shear tests for the core structures were to determine their strength and modulus parallel to the plane of sandwich. The tests were conducted solely on the core material bonded to the thick loading plates. This method provides the load-deflection behaviour of core structures when loaded parallel to the facings. However, this method of testing does not produce pure shear as the secondary forces acting normal to the faces are present, but the prescribed specimen geometry and fixture set up reduce their effects on the obtained results. Test specimen dimensions were decided according to the ASTM recommendations as the three unit cells height were within the 10 mm envelope, the 120 mm long core met the 12 times thickness minimum requirement and 60 mm width. The core adhesion to the steel plate was achieved using Araldite epoxy on the plate in the 50:50 by weight mixture and cured at 50°C for 4 hours to obtain the optimum lap shear strength. The external load applied on the shear test rig produces a rotation of the steel plates that causes secondary peeling stresses at the interface with the core. Since the desired failure mode is 100% shear, specimen experiencing cohesive failures were rejected. Tensile load was applied on the rigid plate through the bolted bracket to the steel plates at crosshead displacement rate of 1 mm/min. **Figure 5** illustrates the details of the testing methods.

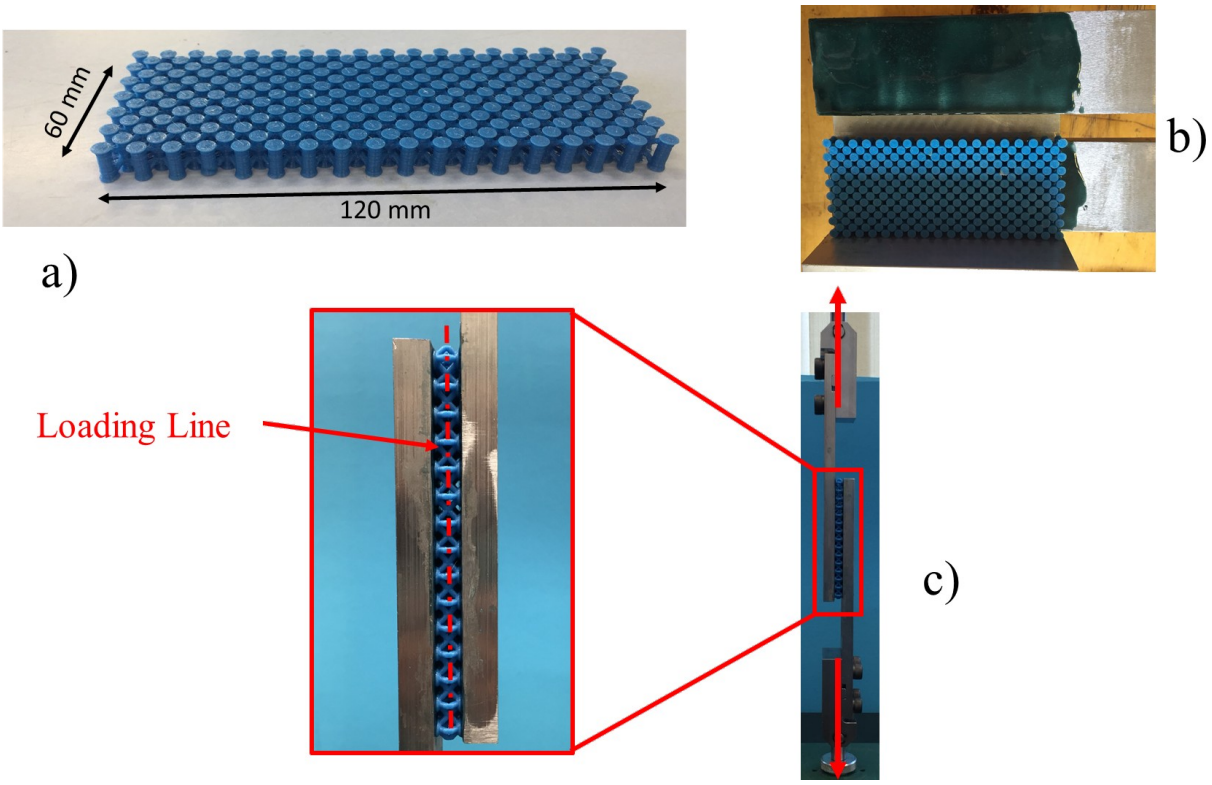

Figure 5 - a) dimensions of the tested core, b) sample preparation, c) test setup and loading direction.

The contact areas of the core lattice structures have an effect on the quality of adhesion to the steel plates. In order to mitigate the premature debonding of the 3-D printed cores from the steel plates, the region adjacent to the bonding surfaces struts were modified. The diameter of the struts was increased only at the ends of the struts to double the contact areas. This modification was not needed for the compressive and flexural tests. The data for load-deflection can be used to derive the effective shear modulus and the ultimate shear strength using:

$$\tau = \frac{P}{Lb} \qquad (1)$$

Where τ, P, L and b are the core shear stress (MPa), load on specimen (N), length of specimen and width of specimen (mm), respectively. Equation 2 uses the specimen geometry and the load-deflection response to derive the shear modulus G of the core:

$$G=\frac{St}{Lb} \qquad (2)$$

Where S and t are the slope of the initial portion of load-deflection curve (N/mm) and thickness of the core (mm).

2.4.4 Flexural testing of sandwich panels

Flexural behaviour of the sandwich structures is affected by the ability of the core shear limits as it undergoes deformation as part of the overall beam displacement. Whereas the facings are responsible for the tensile and compressive load carrying providing directional stiffness and strength while being protected by the core against local buckling. Three-point bending tests were conducted on the NF/ 3DP core sandwich panels according to ASTM C393-06 to determine their flexural properties. A Tinius Olsen testing machine equipped with 25 kN load cell was used to perform the bending tests with a loading rate of 1mm/min. Sample preparation using the 3-D printed lattice cores permanently bonded to the NF face sheets with Araldite 2015 epoxy resin in a 50:50 by weight mixture. Specimens with dimensions of 160 mm length, 40 mm width and overall thickness of 12 mm were put under testing with a setup of span length of 125 mm, support and loading nose radius of 5 mm as illustrated in **Figure 6**. The NF face sheets were cut off a panel using a laser cutter in the above-mentioned dimensions and 2 mm thickness. To avoid indentation failure within the face sheets a face to core ratio of 1:5 was adopted [43]. Sandwich beams were then placed in the oven for 4 hours for curing. The load F and the crosshead displacement were recorded. Force-deflection curves were plotted, and subsequently flexural stiffness and failure loads were determined. Three pieces of specimen per test condition were tested in room temperature 23 ± 2°C and 50 % humidity.

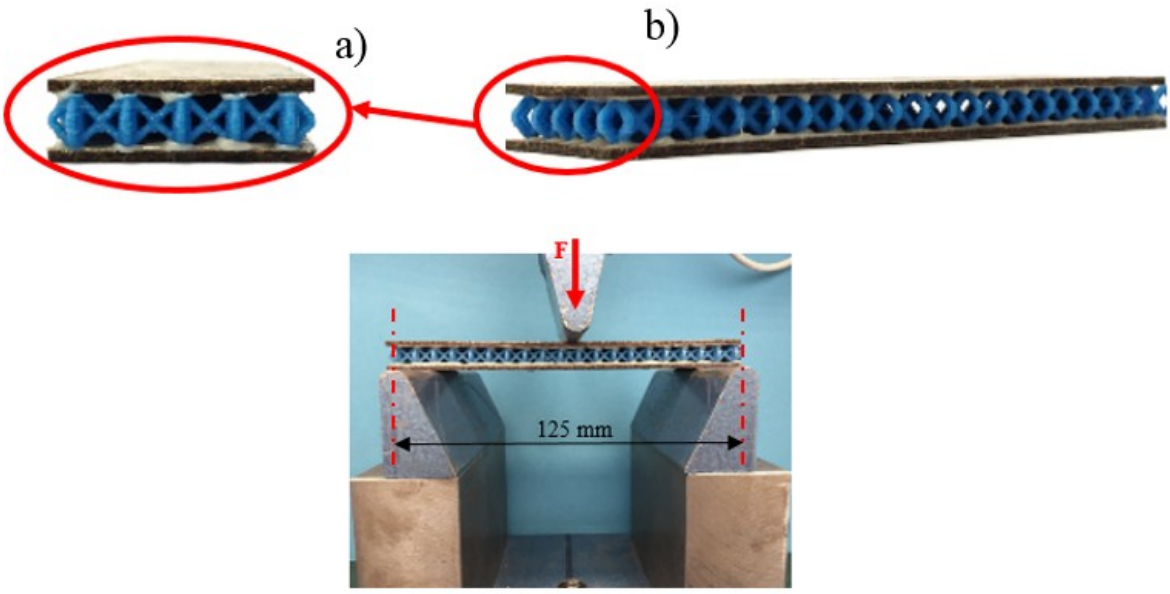

Figure 6 - a) Specimen with lattice core bonded to the NFC skins, b) sandwich panel flexural test set up.

The loading mechanism in terms of nose location with respect to the internal geometry of the core structure had an effect on the obtained results. In particular, a different effect was observed when the moving nose was placed directly on a vertical strut or when it was placed between two inclined struts, which was only a concern within Lattice 1 and 3. The effect of this positioning was quantified in the analysis.

3 Results and discussion

3.1 Tensile results of NFC

Figure 7a) shows the tensile stress vs strain curves of the flax reinforced PP. It is clear that the behaviour of such material is heavily nonlinear as the tangent modulus reduces with increased strain. Three specimens were tested under the same conditions and produced repeatable results in terms of stiffness and strength. The failure of samples was initiated by matrix cracking due to increased strain, which consequently promoted the gradual decrease

in stiffness after 0.5 % strain. Also a closer look at the failed highlighted area in **Figure 7b**, it can be clearly seen the partial failure of flax fibres under tension, which explains the extended load curve to strain exceeding 2 %. The calculated Young's modulus on the initial part of the slope revealed behaviour of an average stiffness value of 1.6 GPa. It has been observed that the strength properties were affected by the fibre content of 52 % as the fibre matrix interface dictates whether the fibre will improve the properties of the composites by transferring the applied load. Fibre distribution and geometry in terms of slenderness ratio also cause local variation of failure mechanisms. The strength of samples was considered as the highest point on the stress-strain curve as an averaged value of 15.2 MPa. The discontinuity and length variation of the flax fibres impede the proper distribution and alignment of load resulting in a shear-like effect hence lower properties. However considering the strain energy demonstrated under the extended curves, few fibres holding the high load for extended strains as observed in **Figure 7a** within the upheld attachment across the failure area.

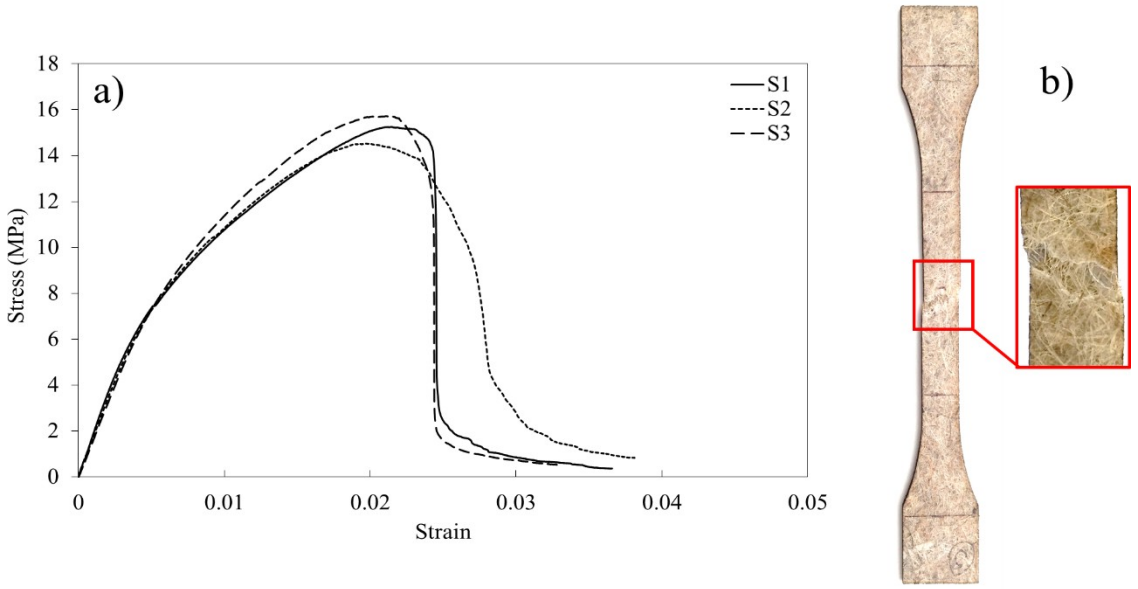

Figure 7 - Tensile test of NFC: a) stress vs strain for three sample repetitions S1, S2 and S3, b) failure area under tension with fibres attached after matrix failure

3.2 Compression results of core lattice structures

The load-displacement curves obtained from testing the three proposed lattice designs under flatwise and edgewise quasi-static compressions are summarised in **Figures 8 and 9** it appears that the internal geometry of the lattice structures affected their behaviour. The responses in all cases were elastic followed by either a plateau as load was maintained for higher displacement as observed within Lattice 1 or a dip of load after reaching the maximum over a longer displacement as observed in Lattices 2 and 3. Lattice 2 represented in **Figure 8b** depicted a variability over the three repeated measurements, which can be explained by the variability of specimen manufacturing as L2_S1 failure mechanisms of its vertical struts as the global buckling is clearly observed in **Figure 8d**.

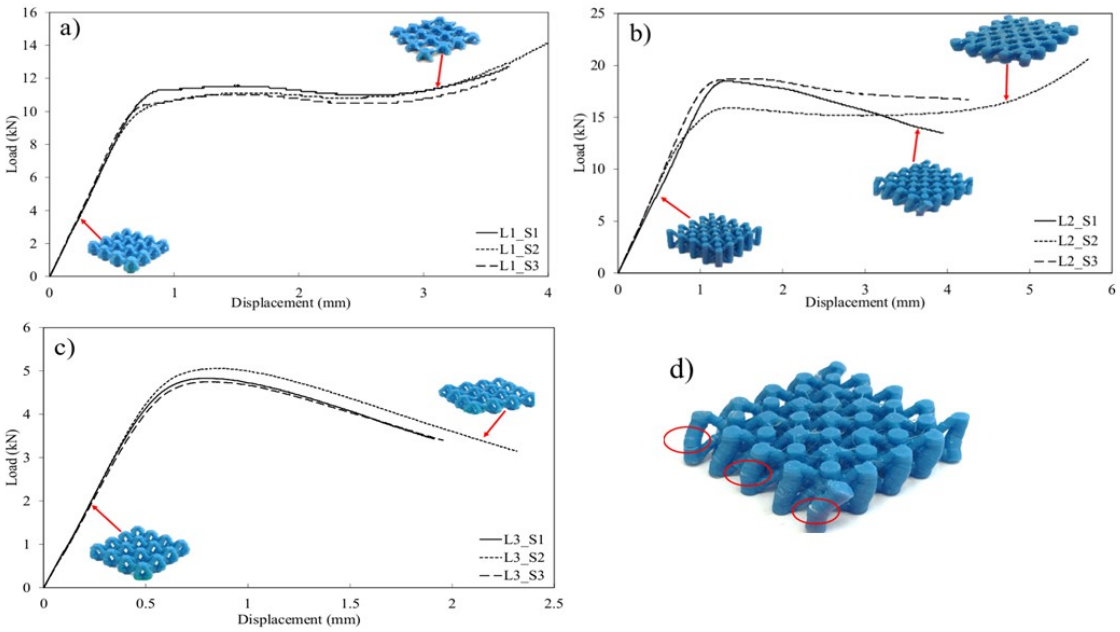

Figure 8 - Load vs displacement curves obtained from the out-of-plane compression test showing the three sample repetitions denoted as S1, S2 and S3: a) Lattice 1, b) Lattice 2, c) Lattice 3 and d) L2_S1 deformation mechanism with vertical struts fracture z.

The stiffness recorded for the three structures was obtained from the slope of the load-displacement curve. It was observed that compressive stiffness of Lattice 1 out-of-plane was 15.5 kN/m whereas the highest stiffness was from Lattice 2 peaked at 18.02 kN/m and the lowest recorded was from Lattice 3 at 8.5 kN/m. The maximum peak load and the stiffness values observed for similar lattice structures reported in literature [44, 45] are comparable to those measured for Lattice 1 and Lattice 2. However, the mechanical behaviour of Lattice 3 is lower than the other two structures, although it is comparable to results reported in literature [46] for metallic cores. An effect of the internal geometry on the mechanical response of the overall structure can be clearly noticed in a way that the vertical struts tend to withstand high compressive loads at higher deformation. This phenomena is then followed by the densification of the struts to act like bulk materials as the load increases at higher displacement. However, in some cases where the printing process has an effect on the performance, the vertical struts tend to buckle under high compressive loads, which explains the relatively maximum load carried by the structure before plummeting with no sign of the densification phase. The buckling mechanism as illustrated in **Figure 8d** initiates at mid-distance through the struts height which then triggers the overall structure sideways collapse. Considering L1, L2 and L3 curves, as shown in **Figure 9**, their performances in terms of stiffness and strength values can be classified in a descending order of L2, L1 then L3 as the crucial contribution of the vertical struts towards the structural integrity was demonstrated.

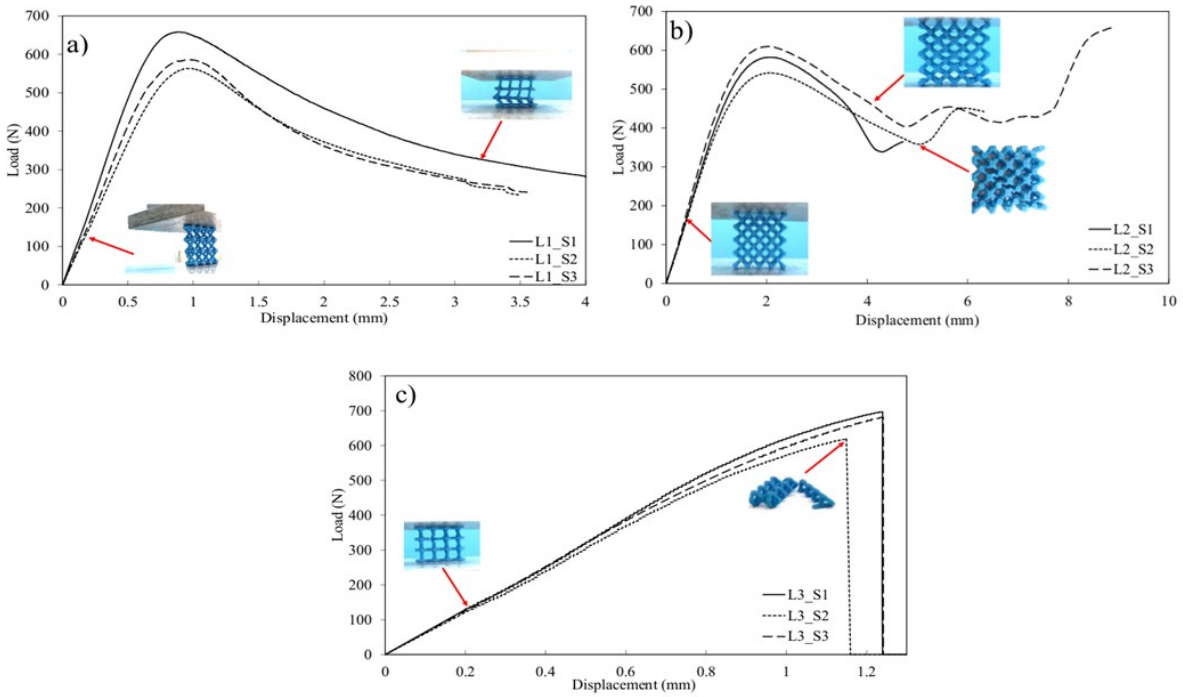

Figure 9 - Load vs displacement curves from the in-plane compression test for the three repetitions with the observed in-situ deformation during and after testing: a) Lattice 1, b) Lattice 2 and c) Lattice 3

The in-plane compression tests performed on the L1, L2 and L3 revealed their structural differences in terms of stiffness and strength in addition to their failure mechanisms. All specimens show typical characteristics of cellular structures exhibiting an elastic response region, yield, plastic strain hardening up to a peak load and post-yield buckling or fracture. Overall the maximum load taken by each structure was much lower compared to the out-of-plane in the range of 500 – 700 N. The in-plane testing direction is normal to the printing direction (i.e. layer by layer, therefore, the interlayer bonding strength is examined). L1 and L2 demonstrated higher strain energy capability as the load was maintained for higher displacement and an apparent ductile failure mechanism through the structure was observed across the three repetitions. In contradiction of L3 for which the failure across all repetitions was consistently brittle with minimal deformation along the displacement direction. This can

be explained by the missing vertical struts, which supplied L1 and L2 with additional support allowing load distribution flowing through the constituents struts of individual unit cells. Lattice 1 samples tend to collapse layer by layer as the connecting struts fold triggering side movements of layers. It can be noticed that the slope and maximum load recorded for the tested specimen showed trivial variability with L1_S1 demonstrated the highest stiffness and strength this can be related to the printing process. Structural imperfections within additively manufactured parts can be categorised into micro-pores or non-uniform diameter of struts which directly affect the deformation mechanism within the lattice structures. Due to the less dense structure of Lattice 1 compared to Lattice 2, an elongated region of diagonal struts buckling before densification of the bottom row of cells was observed as illustrated in **Figure 10a.** Apart from Lattice 3 in which minimal deformation due to the post-yield hardening, which occurred at low strains followed by a sharp drop of load signifying a brittle fracture, Lattice 1 and 2 displayed shear band regions due the broken diagonal struts in the vertices, these are shown in **Figure 10b**. Shear band formation due to bending of the diagonal struts results in the formation of plastic hinges.

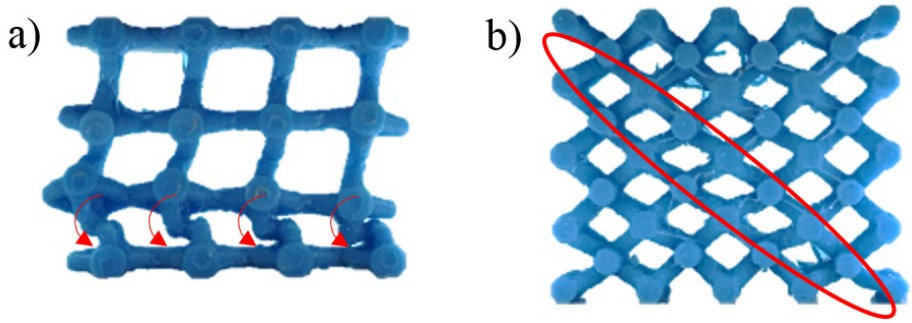

Figure 10 - Deformation mechanisms of lattice structures under in-plane compression tests: a) Lattice 1 shows layer by layer collapse through node rotation, b) Lattice 2 shear band formation with stretch dominant deformation of bottom layer.

3.3 Shear results of core lattice structures

The shear experiments provide the equivalent stiffness and strength of the different core structures with their consequent failure modes. The increased contact surface between the 3D Printed core and the platens improved the adhesion strength and reduced the debonding effects induced due to the minimal bending effects. Common failure locations for all three lattice structures within strut joints as intersection points represent the weakest link of the structure as illustrated in **Figure 11.** Consistent results for all tests in terms of stiffness through load vs displacement slope repeatability, responses in all three configurations were linear elastic followed by either a brittle failure (Lattice 2 and 3) or gradual load drop at increasing strains. The shear strength and modulus have been computed from the experimental results using equation (1) and (2) and the apparent cross section area. It can be seen that Lattice 2 exhibited the highest shear capabilities with maximum taken load of 16 kN equivalent to a shear strength of 2.3 MPa and shear modulus of 17.8 MPa. The sharp load drops within Lattice 2 and 3 after 1.5 mm displacement signify the brittle failure of the overall structure at its critical connection points compared to the elongated displacement for Lattice 1 up to 3 mm with gradual loss of strength. Comparing the obtained results which are summarised in **Figure 11d**, it can be clearly noticed that the slope and maximum load (i.e. stiffness and strength) are affected by the internal topology of each lattice structure. The vertical struts within Lattice 1 provide structural stability under shear loading as the shear modulus is maintained at 17.8 MPa and a slight reduction of strength to 2 MPa as progressive failure of inclined struts under excessive bending causes the immediate load drop

with a tensile failure of connecting struts between adjacent unit cells. **Figure 11b** explains the overall response of Lattice 2 as the high load capacity is owed to the vertical struts taking most of it, but as the connecting struts within individual cells fail under a combined tensile and compressive modes, a subsequent abrupt load drop is associated with a harmonised layer slide closer to the moving platens parallel to the loading plane. Although the similar features between Lattice 1 and 3 apart from the missing vertical strut, it is evident that Lattice 3 suffered a reduced shear strength and modulus of 1.7 MPa and 15.5 MPa respectively as the individual cells shifted along the displacement direction through the dislocation of the weakest link at the intersecting node (**Figure 11c**). In addition to the latter, an evident rotation of diagonal struts as rupture occurs at both upper and lower nodes due to excessive bending.

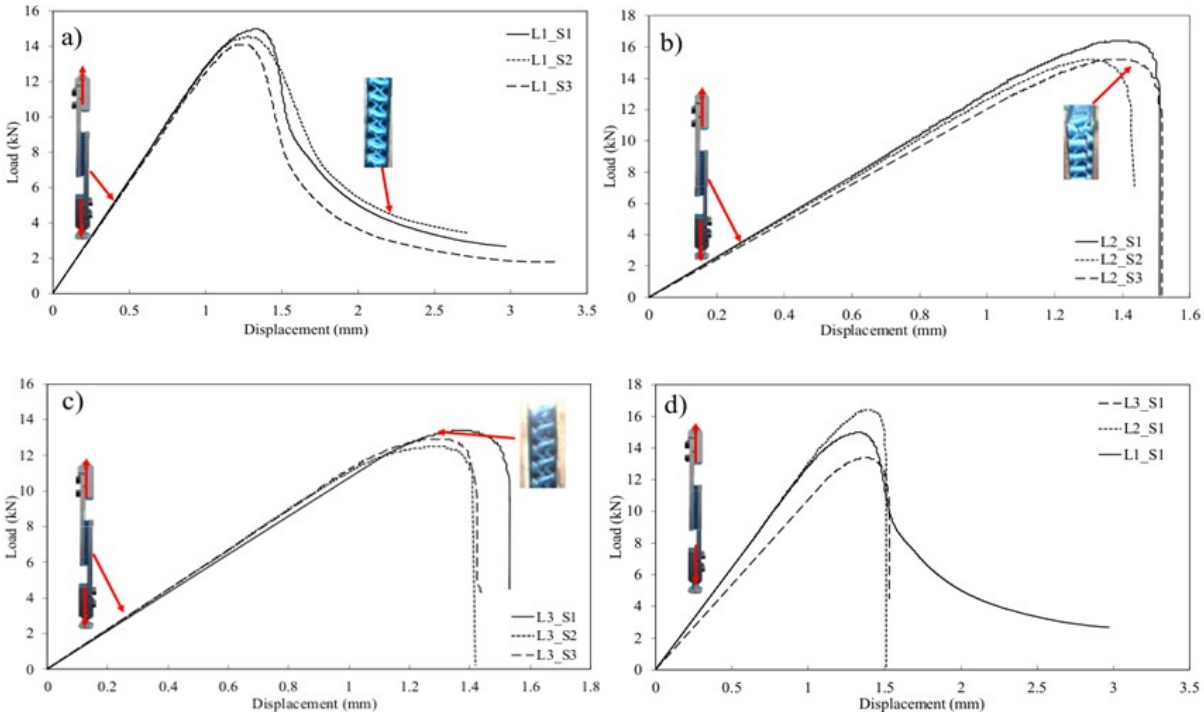

Figure 11 - Load vs displacement curves from the shear test of bonded core lattice: a) Lattice 1, b) Lattice 2, c) Lattice 3 and d) Comparison of the three structures.

Deformation mechanisms of the three core lattice structures under shear loading showing the collapse and fracture of the struts are illustrated in **Figure 12**: **a)** Lattice 1 the vertical strut provides high stiffness and extended deformation within the plastic region as ductile failure was demonstrated, **b)** Lattice 2 clear, brittle failure as sharp cuts develop through the thickness, **c)** Lattice 3 decreased stiffness and lower shear load resistance as top and bottom nodes show a brittle fracture,

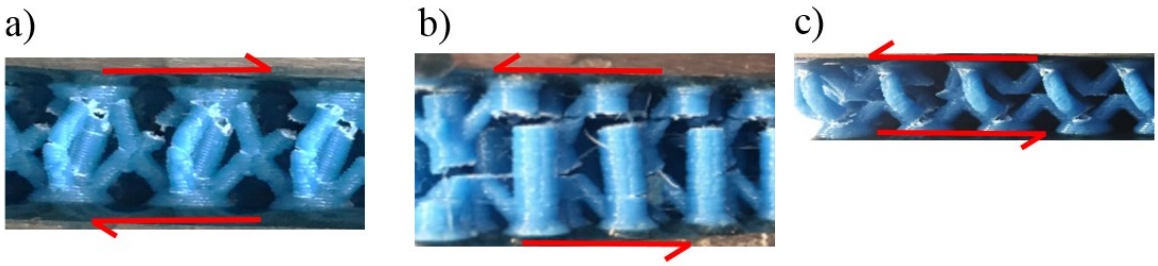

Figure 12 - Failure mechanisms of the three core lattice structures under shear: a) Lattice 1, b) Lattice 2, c) Lattice 3.

3.4 Flexural results of sandwich panels

Having investigated the compression and shear behaviour of the 3D Printed core structures, the obtained results provide an insight into the significance of bending loads on the sandwich structure. In flexural testing, the applied bending moment and transverse shear load are distributed between the constituents of a sandwich panel (i.e. face-sheets and core, respectively). **Figure 13** illustrates the load vs deflection under the flexural test; three specimens have been tested under the same conditions to ensure the findings integrity. However, tests revealed inconsistency as testing of one lattice structure showed diverging responses in terms of flexural strength and plastic strains after the post yielding point.

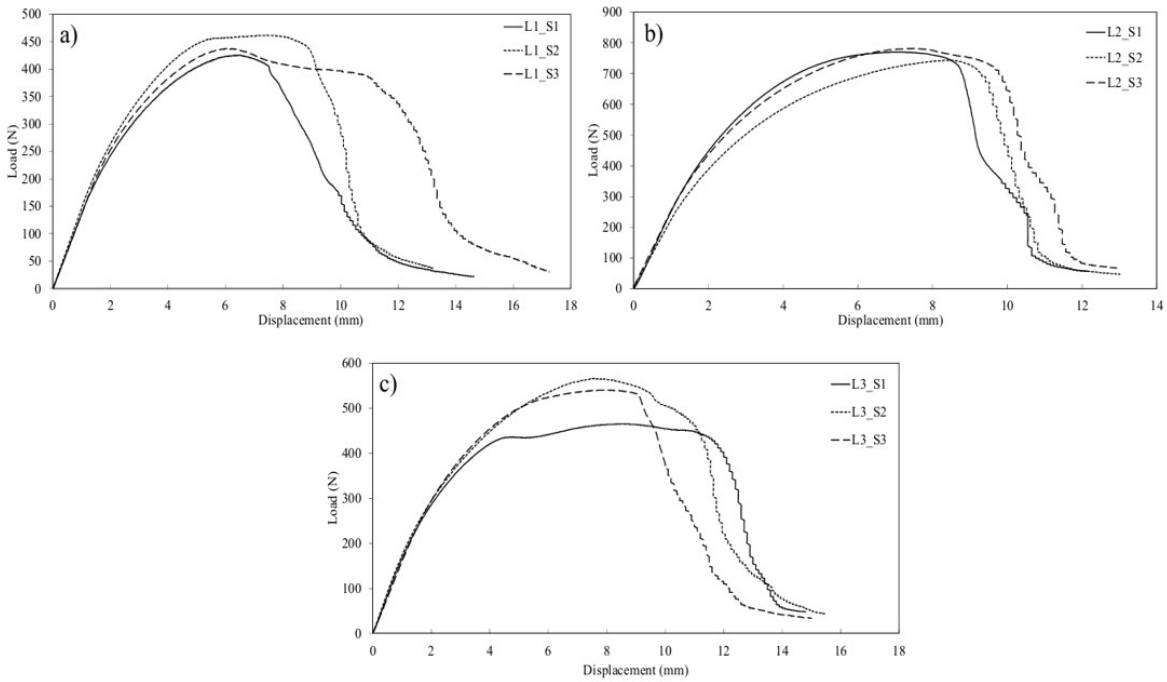

Figure 13 - Bending characteristics of sandwich panels shown on the load vs displacement. Three sample repetitions to show repeatability: a) Lattice 1, b) Lattice 2 and c) Lattice 3

The overall response of the all cell topologies was consistently highly nonlinear as the initial portion of the curve represented the flexural rigidity of the sandwich panel up to a

displacement of ~2 mm. The sandwich panels continue to withstand increasing loads under high plastic deformations beyond the elastic limit point up to a crosshead displacement of ~10 mm. It has been observed that the failure mechanism and flexural strength have been affected by the moving nose placement with respect to the internal geometry of the lattice structure.

In a set up in which the moving load is placed directly on a unit cell, an increased load-bearing capacity was observed with minimal deflection and consequent tensile failure of bottom face-sheet. Whereas if the load is applied over the intersecting node of two adjacent cells, compression of the top face-sheet initiated folding into a V-like shape promoting the panel energy absorption at the cost of its flexural strength. Despite the latter, the stiffness have not been affected in which repeatability was validated by the consistent initial slope. The averaged stiffness values recorded for L1, L2 and L3 were 142, 242 and 162 kN/m, respectively. Good skin-core adhesion was observed throughout all tested specimens as no evidence of delamination was observed, which implies that it can be eliminated as a variable to understand the performance.

Figure 14a shows Lattice 1 (L1_S1) local dislocation of the diagonal strut along the loading line due to stretching whereas the bottom face-sheet exhibited tensile fracture. The maximum load of this particular test was 425 N, which was considered lower than L1_S2 (**Figure 13a**) exhibiting 462 N as the top face-sheet wrinkles at increasing deflection and maintained load. L1_S3 experienced similar response to L1_S1 at a maximum load held within an equivalent deflection region ~6.3 mm, however beyond 8 mm deflection load

dropped through two stages. This dissimilarity can be explained by higher strength of the bottom face-sheet as the tensile fracture was less severe within L1_S3, hence the strut dislocation distance. The progressive diagonal struts failure along the panel width on the normal plane to **Figure 14** is associated with the near plateau load before the sharp drop of load. Results obtained from Lattice 2 tests were consistent in terms of the high stiffness and maximum load as well as the failure mechanism due to its dense topology. This has also reduced the wrinkling effect of the top face-sheet and promoted the tensile fracture of the bottom face and struts dislocation at significantly higher loads ~765 N due to the relatively highly packed structure with vertical struts. Geometrical differences between L1 and L3 being the missing central vertical strut and increased diameter of all struts provided the latter with slightly improved stiffness and strength. The results reported in our paper are in coherence with several studies on the failure mechanisms of the sandwich structures components [47-49]. Although the reported studies focused on metallic truss cores, the parameters affecting the experimental programme are the same. Moreover, Zok et al [50] developed mechanism maps for possible failures of pyramidal metallic truss cores based on beam theory with respect to face and core dimensions.

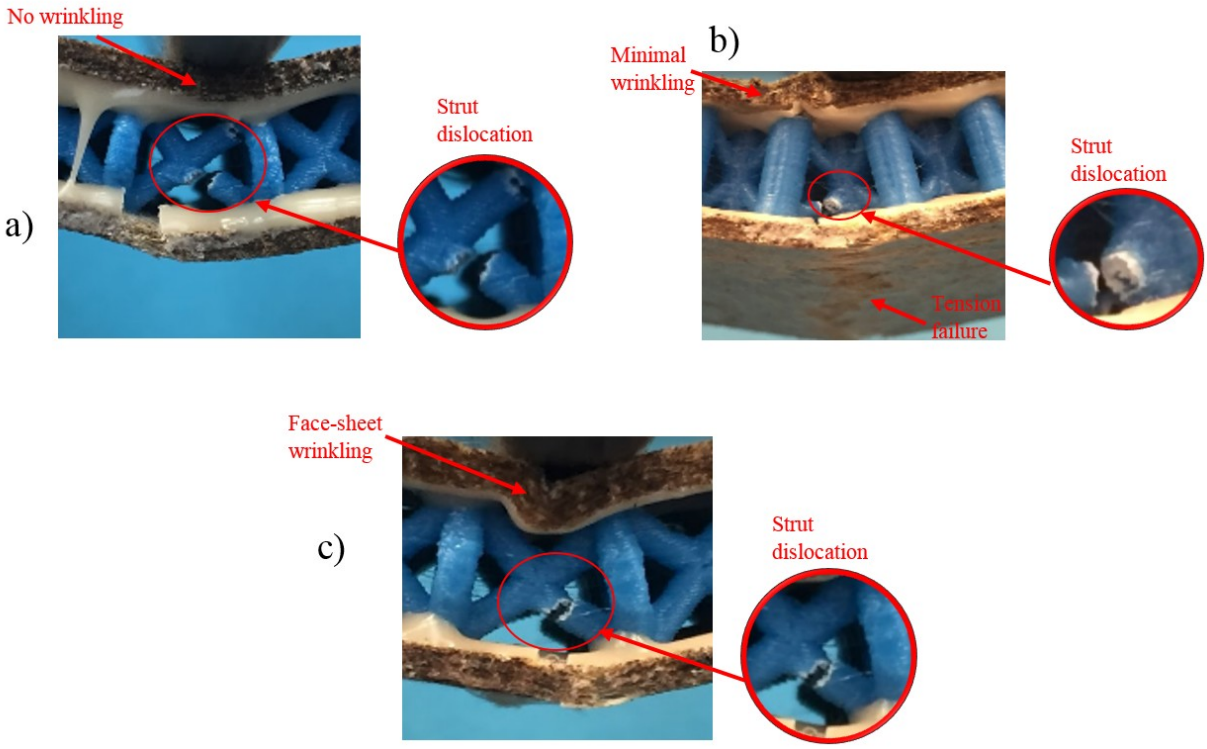

Figure 14 - Deflection and failure mechanisms under bending loading: a) Lattice 1, b) Lattice 2, c) Lattice 3.

In the past, many researchers have studied the potential use of AM lattice structures for various applications [51-54]. Yoon et al. [55] investigated the compressive strength and modulus of 3-D printed ABS engineered trabecular bone and honeycomb biomimetic structures. Results proved that 3DP technology could be an efficient technique for comparative studies. Lee and Kang [56] carried out an experimental analysis on the compressive behaviour of woven Kagome stainless steel wires as a periodic cellular metal structure within two steel face sheets; they found that as the number of layers increases along the out of plane direction the strength decreases. In order to study the effects of variation in strut diameter on the compressive elastic modulus and collapse stress of cellular lattices, Ravari et al. [57] fabricated PLA lattice structures using FFF for the mechanical

characterisation and also developed beam and solid elements based FEM. To achieve realistic elastic modulus and strength each strut needed to be divided into ten and twelve equally spaced intervals respectively. The results found in this study compliment these past works as they can be used to predict mechanical properties of appropriately modelled sandwich structures.

The maximum load values obtained from averaging the three maximum loads recorded from samples repetitions have been normalised with the nominal weight and reported in Table 2. From the comparison, the diamond structure with vertical strut (Lattice 1) performs the best in compression out of the plane and shear whilst the diamond structure without vertical strut (Lattice 3) performs better under compression in plane and three-point bending load. However, the latter diamond structure was modified increasing the diameter of the struts from 1.5 mm to 2 mm. This change justifies the increase in normalised maximum load for the in-plane and the flexural since for the diagonal struts are primarily contributing to the bending and in-plane strength of the cell.

Table 2 - Maximum load values normalised with the nominal weight.

	Normalised maximum load* F/m (N/g)		
	Lattice 1	Lattice 2	Lattice 3
Compression out-of-plane	5090	5000	2306
Compression in-plane	290	164	368
Shear	830	533	724
Flexural	32	26	34

These results are promising. However, there are several limitations to this study that can be improved in future work. First, the top and bottom sheets made of the PP-flax

composite were different materials than the struts (PLA), and they were held together with an adhesive. Although no delamination occurred in testing, and therefore the results are reliable, this introduces as suboptimal method of assembly and materials mixing into the final sandwich structure. As both NF PLA composites have been previously investigated and PP 3-D is possible, it would be interesting to investigate single material sandwich structures of both PP+flax and PLA+flax in the future. To make this realistic from a manufacturing perspective, the lattice structures could be printed in a multi-head 3-D printer [58] using the sheets as substrates. The final layer of the sandwich could be bonded thermally or with adhesives. In addition, the lattice structures were fabricated using relatively thin layers using a high-resolution nozzle that is inadequate for timely manufacturing. Future work should investigate large layer thicknesses from a large nozzle to enable rapid manufacturing of bio-composite sandwich structures. Finally, work should expand applications beyond flat bio-compatible sandwich panels with natural fibre composite skins to more advanced shapes where the skin itself could be 3-D printed.

4 Conclusions

In this paper, FFF technology was used to manufacture lattice structures used as a core for biocompatible sandwich panels with natural fibre composite skins. The mechanical properties of 3DP PLA cores under compression both in-plane and out-of-plane, shear and flexural of the bio-sandwich panel have been carried out. The key findings established in this work are listed as follow:

- A comparison between the investigated geometries shows that the diamond structure with vertical strut (Lattice 1) performs the best in compression out of the plane and shear whilst the diamond structure without vertical strut (Lattice 3) performs better under compression in plane and three-point bending load. The better response for the diamond structure was achieved through modifying the diameter of the struts from 1.5 mm to 2 mm since the diagonal struts are primarily contributing to the bending and in-plane strength of the cell.
- The tensile tests on the natural fibre showed that the failure was ductile with matrix failure first followed by stretching of the fibres until complete failure.
- The failure mechanisms of the core structures observed under the different loading conditions have been discussed. Under compression, in-plane shear band and rotation of the struts have been observed. For the compression out of plane, the main mechanism is plastic hinges followed by densification. In some cases buckling of the vertical struts has been noted. Under shear load, the failure generally occurred at the nodes where the diagonal struts intersect the vertical strut. In addition for the diamond structure without vertical strut, the failure also starts in the middle plane at the intersect node. Under flexural load, the failure always appeared in one of the lower diagonal struts closer to the middle plane under tension load.
- On the basis of the experimental results, the three shapes investigated are well suited for impact applications because of the high shear and out of plane compression strength.

- The experimental results discussed in this work prove the feasibility of AM technology in the process of manufacturing lightweight polymer-based sandwich panels for structural applications. Based upon experimental results this category of core structures could compete with high performing honeycomb structures used for aerospace applications. However, as quality assurance of parts produced with this technology, repeatability is still an issue to be addressed.

Acknowledgements

The authors wish to thank Dr. Anatolii Babutskyi and Mr. Jamie Harrison for the support provided for the testing activities presented in this work and for partial support from the Richard Witte Endowment.

References

[1] H. N. Wadley, N. A. Fleck, and A. G. Evans, "Fabrication and structural performance of periodic cellular metal sandwich structures," *Composites Science and Technology,* vol. 63, pp. 2331-2343, 2003.

[2] G. R. Villanueva and W. Cantwell, "The high velocity impact response of composite and FML-reinforced sandwich structures," *Composites Science and Technology,* vol. 64, pp. 35-54, 2004.

[3] S. Nemat-Nasser, W. Kang, J. McGee, W.-G. Guo, and J. Isaacs, "Experimental investigation of energy-absorption characteristics of components of sandwich structures," *International journal of impact engineering,* vol. 34, pp. 1119-1146, 2007.

[4] J. Shafizadeh, J. Seferis, E. Chesmar, and R. Geyer, "Evaluation of the in-service performance behavior of honeycomb composite sandwich structures," *Journal of Materials Engineering and Performance,* vol. 8, pp. 661-668, 1999.

[5] A. S. Herrmann, P. C. Zahlen, and I. Zuardy, "Sandwich structures technology in commercial aviation," in *Sandwich structures 7: Advancing with sandwich structures and materials*, ed: Springer, 2005, pp. 13-26.

[6] A. P. Mouritz, E. Gellert, P. Burchill, and K. Challis, "Review of advanced composite structures for naval ships and submarines," *Composite structures,* vol. 53, pp. 21-42, 2001.

[7] M. Dweib, B. Hu, A. O'donnell, H. Shenton, and R. Wool, "All natural composite sandwich beams for structural applications," *Composite structures,* vol. 63, pp. 147-157, 2004.

[8] J. F. Davalos, P. Qiao, X. F. Xu, J. Robinson, and K. E. Barth, "Modeling and characterization of fiber-reinforced plastic honeycomb sandwich panels for highway bridge applications," *Composite structures,* vol. 52, pp. 441-452, 2001.

[9] C. B. Williams, J. K. Cochran, and D. W. Rosen, "Additive manufacturing of metallic cellular materials via three-dimensional printing," *The International Journal of Advanced Manufacturing Technology,* vol. 53, pp. 231-239, 2011.

[10] F. Brenne, T. Niendorf, and H. Maier, "Additively manufactured cellular structures: Impact of microstructure and local strains on the monotonic and cyclic behavior under uniaxial and bending load," *Journal of Materials Processing Technology,* vol. 213, pp. 1558-1564, 2013.

[11] N. A. Meisel, C. B. Williams, and A. Druschitz, "Lightweight metal cellular structures via indirect 3D printing and casting," in *Proceedings of the International Solid Freeform Fabrication Symposium*, 2012, pp. 162-176.

[12] L. Yang, "Experimental-assisted design development for an octahedral cellular structure using additive manufacturing," *Rapid Prototyping Journal,* vol. 21, pp. 168-176, 2015.

[13] M. Rashed, M. Ashraf, R. Mines, and P. J. Hazell, "Metallic microlattice materials: A current state of the art on manufacturing, mechanical properties and applications," *Materials & Design,* vol. 95, pp. 518-533, 2016.

[14] H. Yazdani Sarvestani, A. H. Akbarzadeh, H. Niknam, and K. Hermenean, "3D printed architected polymeric sandwich panels: Energy absorption and structural performance," *Composite Structures,* vol. 200, pp. 886-909, 2018/09/15/ 2018.

[15] B. G. Compton and J. A. Lewis, "3D-printing of lightweight cellular composites," *Advanced materials,* vol. 26, pp. 5930-5935, 2014.

[16] D. N. Saheb and J. P. Jog, "Natural fiber polymer composites: a review," *Advances in Polymer Technology: Journal of the Polymer Processing Institute,* vol. 18, pp. 351-363, 1999.

[17] K. L. Pickering, M. A. Efendy, and T. M. Le, "A review of recent developments in natural fibre composites and their mechanical performance," *Composites Part A: Applied Science and Manufacturing,* vol. 83, pp. 98-112, 2016.

[18] K. Van de Velde and P. Kiekens, "Effect of material and process parameters on the mechanical properties of unidirectional and multidirectional flax/polypropylene composites," *Composite structures,* vol. 62, pp. 443-448, 2003.

[19] L. Yan, N. Chouw, and K. Jayaraman, "Flax fibre and its composites–A review," *Composites Part B: Engineering,* vol. 56, pp. 296-317, 2014.

[20] B. T. Wittbrodt, A. Glover, J. Laureto, G. Anzalone, D. Oppliger, J. Irwin*, et al.*, "Life-cycle economic analysis of distributed manufacturing with open-source 3-D printers," *Mechatronics,* vol. 23, pp. 713-726, 2013.

[21] A. Lanzotti, M. Grasso, G. Staiano, and M. Martorelli, "The impact of process parameters on mechanical properties of parts fabricated in PLA with an open-source 3-D printer," *Rapid Prototyping Journal,* vol. 21, pp. 604-617, 2015.

[22] B. Tymrak, M. Kreiger, and J. M. Pearce, "Mechanical properties of components fabricated with open-source 3-D printers under realistic environmental conditions," *Materials & Design,* vol. 58, pp. 242-246, 2014.

[23] M. Grasso, L. Azzouz, P. Ruiz-Hincapie, M. Zarrelli, and G. Ren, "Effect of Temperature on the Mechanical Properties of 3DPrinted PLA Tensile Specimens," *Rapid Prototyping Journal,* vol. 25, 2018.

[24] B. Wittbrodt and J. M. Pearce, "The effects of PLA color on material properties of 3-D printed components," *Additive Manufacturing,* vol. 8, pp. 110-116, 2015.

[25] I. S. T. Heikkinen, Kauppinen, C., Liu, Z., Asikainen, S.M., Spoljaric, S., Seppälä, J.V., Savin, H., Pearce, J.M., "Chemical Compatibility of Fused Filament Fabrication-based 3-D Printed Components with Solutions Commonly Used in Semiconductor Wet Processing. Additive Manufacturing."

[26] A. Le Duigou, M. Castro, R. Bevan, and N. Martin, "3D printing of wood fibre biocomposites: From mechanical to actuation functionality," *Materials & Design,* vol. 96, pp. 106-114, 2016.

[27] S. A. Hinchcliffe, K. M. Hess, and W. V. Srubar, "Experimental and theoretical investigation of prestressed natural fiber-reinforced polylactic acid (PLA) composite materials," *Composites Part B: Engineering,* vol. 95, pp. 346-354, 2016.

[28] R. T. L. Ferreira, I. C. Amatte, T. A. Dutra, and D. Bürger, "Experimental characterization and micrography of 3D printed PLA and PLA reinforced with short carbon fibers," *Composites Part B: Engineering,* vol. 124, pp. 88-100, 2017.

[29] X. Wang, M. Jiang, Z. Zhou, J. Gou, and D. Hui, "3D printing of polymer matrix composites: A review and prospective," *Composites Part B: Engineering,* vol. 110, pp. 442-458, 2017.

[30] Y. Tao, H. Wang, Z. Li, P. Li, and S. Q. Shi, "Development and application of wood flour-filled polylactic acid composite filament for 3D printing," *Materials,* vol. 10, p. 339, 2017.

[31] A. M. Pringle, M. Rudnicki, and J. Pearce, "Wood furniture waste-based recycled 3-D printing filament," *Forest Products Journal,* 2017.

[32] S.-H. Ahn, M. Montero, D. Odell, S. Roundy, and P. K. Wright, "Anisotropic material properties of fused deposition modeling ABS," *Rapid prototyping journal,* vol. 8, pp. 248-257, 2002.

[33] A. R. Torrado, C. M. Shemelya, J. D. English, Y. Lin, R. B. Wicker, and D. A. Roberson, "Characterizing the effect of additives to ABS on the mechanical property anisotropy of specimens fabricated by material extrusion 3D printing," *Additive Manufacturing,* vol. 6, pp. 16-29, 2015.

[34] J. J. Laureto and J. M. Pearce, "Anisotropic mechanical property variance between ASTM D638-14 type i and type iv fused filament fabricated specimens," *Polymer Testing,* vol. 68, pp. 294-301, 2018.

[35] T. D. Ngo, A. Kashani, G. Imbalzano, K. T. Q. Nguyen, and D. Hui, "Additive manufacturing (3D printing): A review of materials, methods, applications and

challenges," *Composites Part B: Engineering,* vol. 143, pp. 172-196, 2018/06/15/ 2018.

[36] A. Bellini and S. Güçeri, "Mechanical characterization of parts fabricated using fused deposition modeling," *Rapid Prototyping Journal,* vol. 9, pp. 252-264, 2003.

[37] W. Tao and M. C. Leu, "Design of lattice structure for additive manufacturing," in *Flexible Automation (ISFA), International Symposium on*, 2016, pp. 325-332.

[38] J. M. Pearce. (2018). *3-D printed truss-like lattice structures.* Available: https://osf.io/mrjzw/

[39] Cura. (08/02/2018). Available: https://ultimaker.com/en/products/ultimaker-cura-software

[40] N. G. Tanikella, B. Wittbrodt, and J. M. Pearce, "Tensile strength of commercial polymer materials for fused filament fabrication 3D printing," *Additive Manufacturing,* vol. 15, pp. 40-47, 2017.

[41] Technical data sheet PLA [Online]. Available: https://docs-emea.rs-online.com/webdocs/1591/0900766b815911d5.pdf

[42] A. Bledzki and A. Jaszkiewicz, "Mechanical performance of biocomposites based on PLA and PHBV reinforced with natural fibres–A comparative study to PP," *Composites science and technology,* vol. 70, pp. 1687-1696, 2010.

[43] K. Kabir, T. Vodenitcharova, and M. Hoffman, "Response of aluminium foam-cored sandwich panels to bending load," *Composites Part B: Engineering,* vol. 64, pp. 24-32, 2014/08/01/ 2014.

[44] C. Mercer, J. Lee, and D. Balint, "An investigation of the mechanical behavior of three-dimensional low expansion lattice structures fabricated via laser printing," *Composite Structures,* vol. 206, pp. 80-94, 2018.

[45] S. Yin, J. Li, B. Liu, K. Meng, Y. Huan, S. R. Nutt*, et al.*, "Honeytubes: hollow lattice truss reinforced honeycombs for crushing protection," *Composite Structures,* vol. 160, pp. 1147-1154, 2017.

[46] R. Mines, S. Tsopanos, Y. Shen, R. Hasan, and S. McKown, "Drop weight impact behaviour of sandwich panels with metallic micro lattice cores," *International Journal of Impact Engineering,* vol. 60, pp. 120-132, 2013.

[47] S. Kazemahvazi, D. Tanner, and D. Zenkert, "Corrugated all-composite sandwich structures. Part 2: Failure mechanisms and experimental programme," *Composites Science and Technology,* vol. 69, pp. 920-925, 2009.

[48] H. Rathbun, Z. Wei, M. He, F. Zok, A. Evans, D. Sypeck*, et al.*, "Measurement and simulation of the performance of a lightweight metallic sandwich structure with a tetrahedral truss core," *Journal of Applied Mechanics,* vol. 71, pp. 368-374, 2004.

[49] H. N. G. Wadley, N. A. Fleck, and A. G. Evans, "Fabrication and structural performance of periodic cellular metal sandwich structures," *Composites Science and Technology,* vol. 63, pp. 2331-2343, 2003/12/01/ 2003.

[50] F. W. Zok, S. A. Waltner, Z. Wei, H. J. Rathbun, R. M. McMeeking, and A. G. Evans, "A protocol for characterizing the structural performance of metallic sandwich

panels: application to pyramidal truss cores," *International Journal of Solids and Structures,* vol. 41, pp. 6249-6271, 2004/11/01/ 2004.

[51] S. Kantareddy, B. Roh, T. Simpson, S. Joshi, C. Dickman, and E. Lehtihet, "Saving weight with metallic lattice structures: Design challenges with a real-world example," in *Solid Freeform Fabrication Symposium (SFF), Austin, TX, Aug*, 2016, pp. 8-10.

[52] D. Mahmoud and M. A. Elbestawi, "Lattice Structures and Functionally Graded Materials Applications in Additive Manufacturing of Orthopedic Implants: A Review," *Journal of Manufacturing and Materials Processing,* vol. 1, p. 13, 2017.

[53] S. Liu, Y. Li, and N. Li, "A novel free-hanging 3D printing method for continuous carbon fiber reinforced thermoplastic lattice truss core structures," *Materials & Design,* vol. 137, pp. 235-244, 2018.

[54] C. G. Ferro, S. Varetti, F. Vitti, P. Maggiore, M. Lombardi, S. Biamino*, et al.*, "A robust multifunctional sandwich panel design with trabecular structures by the use of additive manufacturing technology for a new de-icing system," *Technologies,* vol. 5, p. 35, 2017.

[55] Y.-J. Yoon, S. K. Moon, and J. Hwang, "3D printing as an efficient way for comparative study of biomimetic structures—trabecular bone and honeycomb," *Journal of Mechanical Science and Technology,* vol. 28, pp. 4635-4640, 2014.

[56] B.-K. Lee and K.-J. Kang, "A parametric study on compressive characteristics of wire-woven bulk Kagome truss cores," *Composite Structures,* vol. 92, pp. 445-453, 2010.

[57] M. K. Ravari, M. Kadkhodaei, M. Badrossamay, and R. Rezaei, "Numerical investigation on mechanical properties of cellular lattice structures fabricated by fused deposition modeling," *International Journal of Mechanical Sciences,* vol. 88, pp. 154-161, 2014.

[58] J. J. Laureto and J. M. Pearce, "Open source multi-Head 3D printer for polymer-metal composite component manufacturing," *Technologies,* vol. 5, p. 36, 2017.